

Observations and analysis of an urban boundary layer and sea breezes during extreme heat events

Gabriel Rios ^{1*}, ^{2*}, Prathap Ramamurthy ^{1, 2}

1. Department of Mechanical Engineering, CUNY City College, New York, New York
2. NOAA Center for Earth System Sciences and Remote Sensing Technologies, New York, New York

Corresponding author: Gabriel Rios (grios001@citymail.cuny.edu)

*** Current affiliation(s):** Department of Mechanical Engineering, CUNY City College, New York, New York; NOAA Center for Earth System Sciences and Remote Sensing Technologies, New York, New York

For submission to the Quarterly Journal of the Royal Meteorological Society.

Last updated: February 15, 2022.

¹ Abstract

² Extreme heat presents a significant risk to human health and infrastructure in cities. Several studies
³ have been conducted in the past several decades to understand the interaction between the synoptic-
⁴ scale extreme heat events and local-scale urban heat island effects. However, observations of boundary
⁵ layer characteristics during these periods have been relatively rare. Our current understanding of urban
⁶ boundary layer structure is incomplete, particularly in coastal environments where the local climatology
⁷ is highly influenced by land-sea thermal gradients. In this study, we analyze the evolution and structure of
⁸ the urban boundary layer during regular and extreme heat periods with the goal of better understanding
⁹ the effect of extreme heat and sea breezes on the boundary layer over a coastal urban area. Our analysis
¹⁰ focuses on the New York City metropolitan area and relies on observations from vertical profilers (Doppler
¹¹ lidar, microwave radiometer) and quantities derived by analytical methods. Additionally, satellite and
¹² reanalysis data are used to supplement observational data. Extreme heat events present a mean peak
¹³ surface temperature increase of 7K, an increase of site-averaged specific humidity at the surface by
¹⁴ 39.4%, and a marked southwesterly shift in winds at all sites. In addition, sea breeze events during
¹⁵ heat extreme heat events are found to reduce temperatures and increase low-level moisture content from
¹⁶ the early evening through nighttime hours, with strong variability between sites. The study also finds
¹⁷ that extreme heat events unify horizontal wind directions throughout the boundary layer, and promote
¹⁸ nocturnal onshore moisture transport.

¹⁹ 1 Introduction

²⁰ Extreme heat poses a major risk to life and property. The effects of extreme heat are expected to
²¹ impact cities especially, which presents a significant hazard for vulnerable populations and infrastructure.
²² With regards to effects on public health, studies have shown that extreme and prolonged heat increases
²³ mortality and exacerbates existing health conditions in high-risk populations (Anderson and Bell, [2011](#);
²⁴ Frumkin, [2016](#); Heaviside, Macintyre, and Vardoulakis, [2017](#); Madrigano et al., [2015](#)). With regards to
²⁵ effects on infrastructure, studies have shown that extreme heat subjects networks critical to urban areas
²⁶ (e.g., electrical grid, public transportation) under significant stresses and/or failure (McEvoy, Ahmed,
²⁷ and Mullett, [2012](#); Zuo et al., [2015](#)). These events are projected to increase in frequency due to the effects
²⁸ of climate change. Projections indicate that the impacts of future climate will cause adverse effects of
²⁹ extreme heat to become more frequent and severe (Burillo et al., [2019](#); Forzieri et al., [2018](#); Peng et al.,
³⁰ [2011](#)).

31 The meteorology of extreme heat events and its impacts on urban areas can be observed from the synoptic
32 and local scales. From a synoptic scale, extreme heat events are often caused by the sustained presence of
33 a high-pressure system over an area, resulting in lower wind speeds and warm air subsidence, promoting
34 higher surface temperatures (Black et al., 2004; Miralles et al., 2014). From a local perspective, the
35 amplified impact of extreme heat events on cities is a result of the urban heat island (UHI) effect,
36 which occurs as a result of the modification of land surface properties due to the built environment.
37 The modification of surface properties has been shown to increase near-surface air temperatures due to
38 factors such as radiation entrapment, increased heat storage, and lower evapotranspirative cooling (F.
39 Chen, Yang, and Zhu, 2014; Dan Li and Elie Bou-Zeid, 2013; Ramamurthy and Bou-Zeid, 2017; Zhao
40 et al., 2018). Additionally, urban areas near large bodies of water experience effects from the sea breeze,
41 which has been shown to play a moderating influence on the intensity of the UHI effect (Hu and Xue,
42 2016; Jiang et al., 2019; Stéfanon et al., 2014). The processes on these two scales can be connected by
43 understanding the structure and dynamics of the urban boundary layer (UBL), which is the lowest part of
44 the troposphere in which surface-atmosphere exchanges occur that directly affect human activity. There
45 have been a large number of numerical studies performed to improve our understanding of UBL processes
46 during extreme heat events, which have been important for conceptualizing the role of synoptic-scale
47 and surface forcings on urban climate. Something about the vertical structure of the UBL and coupling
48 these

49 However, detailed observational analyses of UBL structure and dynamics are somewhat limited, especially
50 in the vertical direction. Over the last 20 years, microwave radiometers, lidars, and radiosondes have
51 been shown to be essential for accomplishing this. Microwave radiometers have been used to determine
52 vertical profiles of temperature and water vapor (Rose et al., 2005; Z. Wang et al., 2012), while lidars
53 being used to observe three-dimensional wind fields and aerosol concentrations (Grund et al., 2001).
54 Although radiosondes provide direct measurements of the aforementioned properties in the boundary
55 layer as it moves vertically through it, they present greater difficulties (e.g., cost, shorter supply) and
56 are unable to observe at the temporal resolution of microwave radiometers and lidars.

57 Although somewhat limited in spatiotemporal scale, numerous observational campaigns have been per-
58 formed to better our understanding of UBL structure and dynamics. Barlow et al. (2011) provides an
59 in-depth study of boundary layer dynamics above London over a month-long period using a combination
60 of a sonic anemometer and Doppler lidar, allowing for high-resolution vertical observations of a complex
61 UBL and a better understanding of turbulent structures and vertical mixing processes. Similarly, Pel-
62 liccioni et al. (2012) employs a sonic anemometer and a sodar system at a site in Rome to observe and
63 analyze the lower 200 m of the UBL to determine UBL characteristics and explore the validity of Monin-
64 Obukhov similarity theory in the surface layer. Additionally, Arruda Moreira et al. (2020) evaluates the
65 ability of lidar and microwave radiometer systems to observe turbulence over a variety of atmospheric
66 conditions, including the effects of significant dust concentrations, in the region around Granada, Spain.
67 Studies such as those performed by Banks et al. (2015), Quan et al. (2013), and Z. Wang et al. (2012)
68 further demonstrate the ability of vertical profiling instruments to analyze the boundary layer structure
69 by deriving UBL heights and its diurnal evolution. Expanding upon UBL structure, Anurose, Subra-
70 hamanyam, and Sunilkumar (2018) details a long-term observational campaign over an urban location
71 in southern India that chronicles UBL height through monsoon season, annual averages of near-surface
72 quantities, and the dynamics and effects of the sea breeze circulation.

73 Observations of the UBL during extreme heat events are even more limited. Ramamurthy and Bou-Zeid
74 (2017) used microwave radiometers to observe the UBL over New York City in July 2016 to find that
75 the UHI effect was amplified during heat wave events and that spatial variability throughout the city
76 was significant throughout the observation period. Jiang et al. (2019) explores the effects of heat waves
77 on rural and urban areas for several cities in China using ground-based observations with a focus on the
78 UHI effect, finding that the effect was amplified during heat waves due to greater surface solar radiation

79 and shifts in wind direction contributing to advection of heated air masses over the studied cities. (Wu
80 et al., 2019) uses a combination of a ceilometer and multiple lidars to observe the evolution of UBL
81 structure, air quality, and pollutant transport during a heat wave in New York City, demonstrating
82 sharp rates of UBL growth due to convective activity and an increase of pollutant concentration and
83 regional transport. Y. Zhang et al. (2020) uses aircraft-based observations to provide a comprehensive
84 analysis of UBL structure during heat wave events over cities in the United States throughout a 10-year
85 period, providing insights into the 'heat dome' thermodynamic structure over cities and the variability
86 between heat wave events due to local (such as surface properties in urban areas) and large-scale (such
87 as synoptic meteorological conditions) forcings.

88 New York City represents a complex case for urban meteorology given its diverse array of land cover
89 types (deciduous forest to supertall skyscrapers) and its proximity to multiple major bodies of water
90 (Lower New York Bay and the New York Bight to the south and east, Long Island Sound to the north
91 and east). Due to these factors, the effects of the surface energy budget (Hrisko, Prathap Ramamurthy,
92 and Gonzalez, 2021; Prathap Ramamurthy and Bou-Zeid, 2014; Tewari et al., 2019) and sea breezes
93 (Childs and Raman, 2005; Colle and Novak, 2010; Frizzola and Fisher, 1963; Gedzelman et al., 2003;
94 Melecio-Vázquez et al., 2018; Thompson, Holt, and Pullen, 2007) on the mesoscale meteorology have
95 been studied extensively. However, similar to studies of other urban areas mentioned previously, much
96 of this research has involved numerical simulations of these meteorological processes. In this study, we
97 attempt to further our understanding of the UBL over a coastal urban area by compiling observations
98 from multiple locations within New York City and analyzing the UBL using derived quantities.

99 This study attempts to use observations and analytical methods to provide insight into the following
100 questions:

- 101 1. How do UBL structure and dynamics depart from the climatology during extreme heat events?
- 102 2. How do extreme heat events impact the transport of scalars?
- 103 3. What effect does the sea breeze have on a coastal urban area during extreme heat events?

104 2 Data collection and analysis

105 2.1 Study site

106 The UBL over New York City is observed and analyzed in this study. Observational data was captured
107 at four locations within New York City (Table 1).

Table 1: Locations and details of observations sites.

	Bronx	Queens	Staten Island
Coordinates	40.87248°N, 73.89352°E	- 73.81585°E	- 74.14850°E
Elevation (m a.g.l.)	57.8	56.3	32.4
Element roughness height (m a.g.l.)			
Valid wind directions	N/A	180 to 360°	N/A

109 2.2 Observational instruments

110 Observations of the UBL were made using a synthesis of microwave radiometers, lidars, and satellites.

111
112 Vertical profiles of temperature and vapor density were captured using a network of Radiomet-
113 rics MP-3000A microwave radiometers (Hewison and Gaffard, 2003) operated by the New York State

114 Mesonet (Brotzge et al., 2020). Profiles for water vapor are retrieved using 21 channels in the 22-30.0
115 GHz (K-band) range, while profiles for temperature are retrieved using 14 channels in the 51-59.0 GHz
116 (V-band) range. Profile accuracy (relative to radiosonde soundings) determined by performance studies
117 at various locations reported an annually-averaged water vapor accuracy within 1.0 g m^{-3} below 2 km
118 and an annually-averaged temperature accuracy within 1.6 K below 4 km (Güldner and Spänkuch, 2001;
119 Sánchez et al., 2013). Quantities are captured at 58 height levels starting at ground level and ending
120 at 10 km above ground level, with vertical steps of 50 m from ground level to 500 m, 100 m from 500 m
121 to 2 km, and 250 m steps above 2 km. Observation integration times range from 0.01 to 2.50 s. Vertical
122 profiles are generated every 10 s and averaged over 10 min periods.

123

124 Wind measurements were measured using a network of Leosphere WindCube 100S Doppler lidars
125 operated by the New York State Mesonet (Brotzge et al., 2020). Measurements of wind motion using
126 the Doppler beam swinging scan mode in three directions: zonal (u), meridional (v), and vertical (w)
127 over 20 s cycles, with measurements averaged over 10 min intervals (Shrestha et al., 2021). The vertical
128 range of the WindCube 100S is 7 km above ground level with wind speed and direction accuracies of
129 0.5 m s^{-1} and 2° , respectively. The WindCube 100S has also been shown to perform with a high degree
130 of accuracy relative to radiosonde soundings, especially above 500 m (Kumer, Reuder, and Furevik, 2014).

131

132 Land and sea surface temperatures were estimated using derived products from the NOAA/NASA
133 GOES-16 Advanced Baseline Imager (ABI) (Ignatov et al., 2010; Yu et al., 2008). The GOES-16 ABI
134 provides a spatial resolution of 2 km with real-time data available to the public on an hourly basis.
135 The spatial extent of the Land Surface Temperature (LST) product ranges from the continental United
136 States (CONUS) to the majority of the Western Hemisphere (known as *full disk*), whereas the Sea
137 Surface Temperature (SST) product has a full disk spatial extent. The LST product has been found
138 to have an error relative to surface observations of 2.5 K over all land cover types, while sea surface
139 temperatures (SSTs) estimated using the GOES-16 ABI have been found to have an error relative to
140 shipborne radiometers $\leq 1 \text{ K}$ in the New York Bight (Luo and Minnett, 2021).

141 2.2.1 Data criteria & availability

142 Dates selected for this study are categorized into three groups: (1) normal days, (2) extreme heat days,
143 and (3) sea breeze days. For the purposes of this study, *extreme heat events* are defined as 3 or more
144 consecutive days with maximum daily temperatures exceeding 90°F (305 K), per the New York branch
145 of NOAA National Weather Service (Robinson, 2001; National Weather Service, 2018), while *normal*
146 *days* are defined as days that do not meet these criteria. Because the aim of this study is to observe the
147 effect of extreme heat on the UBL, normal day selection was restricted to months in which extreme heat
148 events occurred (May through September), as well as days in which 50% or more of the day featured
149 clear-sky conditions below 3.65 km above ground level due to the association of extreme heat events with
150 reduced daytime cloud coverage and precipitation (Stéfanon et al., 2014; Thomas et al., 2020). Clear-
151 sky conditions were identified by using an average of 5-minute surface-based observations from three
152 airports in the Automated Surface Observation System (ASOS) (NOAA et al., 1998) network within
153 the New York City metropolitan area: Newark Liberty International Airport (EWR), John F. Kennedy
154 International Airport, and LaGuardia Airport. *Sea breeze events* are identified as times during normal
155 and extreme heat days in which the low-level ($\leq 200 \text{ m}$) mean horizontal wind speed (U) is less than
156 5 m s^{-1} and low-level wind direction has a primarily easterly component, due to the presence of the
157 Atlantic Ocean to the east of New York City.

158 - Discuss quality filtering - Plots showing sampling counts per hour per site per day

159 **2.3 Derived quantities**

160 **3 Normal and extreme heat boundary layer properties**

161 This section discusses the differences in boundary layer structure and properties between normal days
162 and extreme heat events. Results are presented from the averages over all identified normal and heat
163 event days.

164 **3.1 Temperature**

165 On average, extreme heat events increase the temperature at the surface, as expected (see Figure
166 4). This is consistent across all observed locations in New York City, with the extreme heat event
167 temperature exceeding normal temperatures by approximately $1-\sigma$ over the entire day. An increase in
168 the difference is observed during daytime hours, with the difference peaking in magnitude around 13:00
169 LST at the hottest time of day. The surface temperature variability is significantly lower during heat
170 events (average $\sigma = 1.77\text{K}$) than during normal temperatures (average $\sigma = 4.57\text{K}$). There is little
171 spatial variability between sites, with maximum average temperatures ranging from 305.65 K in Queens
172 to 306.63 K in the Bronx. It is worth noting that there are areas in New York City that are located
173 in more heavily urbanized areas than the observation sites (such as Midtown Manhattan and central
174 Brooklyn), so it is likely that certain areas within the city have higher maximum temperatures.

175
176 Above the surface, extreme heat events increase the temperature significantly over the lowest
177 3000 m of the troposphere (see Figure 3), with standardized anomalies of θ ranging from $\sigma = 0.99$ to
178 1.30. The largest temperature anomalies shift from the surface layer in the mornings to span the entirety
179 of the mixed layer. This is reflective of strong surface forcing resulting in convection through the mixed
180 layer, as indicated by the formation of a late morning superadiabatic layer at all locations (Figures 5, 6, 7).

181
182 These vertical profiles of θ suggest a degree of spatial variability in the UBL exists between loca-
183 tions. One instance of this spatial variability is vertical mixing; the Bronx site appears to have
184 stronger vertical mixing as shown in Figure 5, as θ remains constant for a greater height than at
185 the Queens and Staten Island locations, indicating a deeper mixed layer. This phenomenon is more
186 pronounced during extreme heat events, as a distinct mixed layer is apparent in the Bronx during early
187 (12:00 LST) and late (18:00 LST) afternoon hours. While a deepened mixed layer during extreme heat
188 events is also visible for the other locations, the strength of vertical mixing in the Bronx is emphasized
189 by persistent afternoon instability as shown by negative $\frac{d\theta}{dz}$ values between 500 and 1000 m and a
190 superadiabatic surface layer and 12:00 and 18:00 LST.

191 **3.2 Moisture**

192 On average, extreme heat events were found to increase the moisture at the surface, as indicated by
193 the diurnal profiles of specific humidity (q) (see Figure 9). This is also consistent across all observed
194 locations in New York City, with the extreme heat event temperature exceeding normal temperatures
195 by approximately $1-\sigma$ over the entire day. Although a distinct diurnal profiles exists (q decreases during
196 daytime hours), the diurnal range is smaller in magnitude than temperature. It is also worth noting
197 that the diurnal range is lower for Staten Island than for the Bronx or Queens, suggesting that degree of
198 urbanization has a negative correlation with the diurnal range of q . Similar to surface temperature, the
199 variability of q is significantly lower during heat events (average $\sigma = 2.14 \times 10^{-3} \text{ kg kg}^{-1}$) than during
200 normal temperatures (average $\sigma = 3.18 \times 10^{-3} \text{ kg kg}^{-1}$). Queens shows exceptional variability in q ,
201 which may be attributed to the location of the observation site, which is adjacent to Flushing Meadows
202 Corona Park (large open vegetated space), is surrounded by a medium-density urban area on all other
203 sides, and is approximately 4 km from Long Island Sound.

204

205 In the boundary layer, the positive q anomalies subside in magnitude between 300 and 600 m,
 206 but increase significantly in the mixed layer, especially during the late morning and early afternoon for
 207 all sites. As shown in Figure 8, the largest anomalies occur between 10:00 and 16:00 LST throughout the
 208 mixed layer. With regards to spatial variation in q , Staten Island demonstrates a strong positive anomaly
 209 overnight through the early morning near the surface, indicating elevated low-level moisture transport
 210 during extreme heat events, whereas the Bronx and Queens demonstrate a similar phenomenon with
 211 a lesser anomaly magnitude. All sites show significant positive q anomalies throughout the day, with
 212 the strongest anomaly signal starting in the low-levels throughout the morning and transitioning to the
 213 mixed later by mid-afternoon. This trend suggests that the increase in nocturnal low-level moisture
 214 corresponds to increased UBL moisture content due to strong vertical mixing throughout the daytime.

215

216 This is supported by Figures 10, 11, 12, where vertical profiles of q across all locations show
 217 markedly higher q values at the surface during extreme heat events with $\frac{dq}{dz}$ values increasing throughout
 218 the morning in the mixed layer while low-level q values decrease, indicating vertical transport of moisture
 219 and drier low-level conditions during peak insolation. The strong vertical mixing of q can be observed
 220 at all sites, where late morning and early afternoon $\frac{dq}{dz}$ values are greater during extreme heat events
 221 than normal days. An example can be seen in the Bronx, where $\frac{dq}{dz} > 0$, indicating very efficient vertical
 222 moisture transport.

223 3.3 UBL dynamics

224 3.3.1 Horizontal winds

225 Extreme heat events coincided with an overall reduction of horizontal wind speeds (U) in the UBL
 226 (Figure 13). More specifically, the magnitude of U during extreme heat events is similar in magnitude
 227 to U during normal days with the exception of early morning hours and at upper levels of the UBL. As
 228 shown in Figure 14, modest reductions in U ($-1.2 \leq \sigma \leq -0.4$) during extreme heat events are present
 229 throughout the UBL from early to mid-morning, with little difference throughout the rest of the day
 230 ($-0.4 \leq \sigma \leq 0.4$). Larger deviations between U values are present at the top of the UBL where synoptic
 231 conditions become dominant.

232

233 Vertical profiles of U for normal and extreme heat events provide a more detailed view of the
 234 differences in UBL structure. Across all sites, U is similar throughout the UBL overnight, afternoon,
 235 and evenings. During early morning hours, however, extreme heat event U values decrease by 25
 236 to 50% throughout the entire UBL (see Figures 15, 16, 17), although both event types present a
 237 classical logarithmic wind profile, with surface friction effects present through 500 m. The reduction
 238 in U during extreme heat events is likely due to the presence of an anticyclonic circulation that
 239 suppresses the nocturnal low-level jet over New York City (T. C. Chen and Kpaeyeh, 1993). Another
 240 phenomenon worth noting is the difference in U profiles above 2000 m; profiles of U during extreme
 241 heat events are more consistent between sites and vertically than during normal days. This phe-
 242 nomenon is the effect of synoptic meteorological conditions on U , as the UBL typically remains below
 243 2500 m. During extreme heat events, anticyclonic conditions produce more consistent atmospheric con-
 244 ditions relative to normal days, resulting in less variability between heat events than during normal days.

245

246 Extreme heat events result in a southwesterly shift in U throughout the UBL. This shift is present most
 247 evidently closer to the surface, as shown in Figures 18, 19, and 20, with winds at 100 m coming primarily
 248 from the southwest quadrant. Figure 19 shows that Queens also presents a secondary maximum with
 249 winds approaching from the south, which suggests effects from the Atlantic sea breeze (effects from
 250 the sea breeze will be further discussed in Section 4). At 1000 m, the directionality of prevailing winds
 251 becomes more uniform between normal and extreme heat days, as winds primarily approach New York

252 City from the west-southwest. The disparity in wind directions between 100 and 1000 m suggests that
253 localized wind fields play a more significant role in UBL dynamics at lower levels whereas synoptic-scale
254 atmospheric conditions increasingly dominate with increasing height. Regardless, the uniformity of
255 wind direction during extreme heat relative to normal days indicates that synoptic-scale effects can
256 play a larger role at lower levels due to advection from the continent, especially with regards to thermal
257 advection that leads to the transport of heated inland air masses over New York City (Ramamurthy, Li,
258 and Bou-Zeid, 2017).

259 3.3.2 Vertical motion

260 On average, extreme heat events do not appear to produce significant changes in vertical velocity (w).
261 Figure 21 shows average diurnal profiles of w at all locations at 100 m above ground level, with similar
262 mean values throughout the day between normal days and extreme heat events. During extreme heat
263 events, however, the variability of w is less in the early morning hours and greater in the evening. This
264 phenomenon is also observed in vertical profiles of w at all locations as shown in Figures 23, 24, and
265 25. At all locations, overnight and morning profiles of w (0:00 and 6:00 LST) show significantly lower
266 variability in w throughout the UBL with similar magnitudes of mean w . Despite similar means and
267 deviations in the early afternoon (12:00 LST), evening profiles (18:00 LST) show significantly higher
268 variability in w below 500 m for all sites, with the Bronx showing this occurrence extend through the
269 UBL. The similarity in vertical profiles of w may be a result of a balance between large-scale subsidence
270 (due to the presence of high-pressure during extreme heat events) and the effects of increased surface
271 forcings during extreme heat events relative to normal days (Dong et al., 2018; D.-L. Zhang, Shou, and
272 Dickerson, 2009).

273 4 Effects of the sea breeze circulation

274 Sea breezes in New York City occur as a result of land-sea temperature gradients from two arms of the
275 Atlantic Ocean; the New York Bight to the southeast and Long Island Sound to the northeast. Sea
276 breezes from both bodies increase the complexity of UBL dynamics over New York City due to the
277 coalescence of opposing fronts over a complex topography (Bornstein and Thompson, 1981). A typical
278 sea breeze event in New York City is defined by calm ambient low-level winds ($\leq 5 \text{ m s}^{-1}$, the formation
279 of a large land-sea temperature gradient in the mid- to late morning, strong late-morning thermals
280 that promote low-level convergence, and afternoon to early-evening onshore moisture transport and
281 reduction in surface air temperatures (especially in areas closest to the shore) (Childs and Raman, 2005;
282 Frizzola and Fisher, 1963; Gedzelman et al., 2003).

283
284 Sea breeze events occurred on approximately 56% of all days observed. The high frequency of
285 occurrence is attributable to low-level convergence due to the large land-sea temperature gradient that
286 is common during warmer months (Childs and Raman, 2005; Gedzelman et al., 2003; Thompson, Holt,
287 and Pullen, 2007), as days were chosen exclusively between May and September. Maximum land-sea
288 surface temperature differences during days with identifiable sea breeze events averaged at 12 K, with a
289 strong diurnal profile with the peak difference occurring around midday (see Figure 26). The frequency
290 of occurrence increases when observing days during extreme heat events, as the lack of a strong synoptic
291 wind allows for the sea breeze circulation to become dominant in the metropolitan area (Miller et al.,
292 2003).

293 4.1 UBL structure during sea breeze events

294 During normal days, observations show that the sea breeze reduces temperatures and increases moisture
295 content throughout the UBL after 12:00 LST. In Figure 27, the standardized anomalies of θ between
296 normal days with and without a sea breeze are shown, averaged over all days for each set of days.

297 Overnight and in the early morning, positive anomalies of θ are present above the UBL (≤ 1 km)
298 until mid-morning, with the Bronx having the most significant anomaly and Staten Island the least.
299 This suggests a decreasing degree of anomalous θ with decreasing urbanization. This anomaly pattern
300 coincides with a positive q anomaly trend in both the spatiotemporal aspect (peak anomaly occurs
301 above 1 km before 8:00 LST) and the magnitude aspect (the Bronx has the most significant early
302 morning anomaly, Staten Island has the least). Later in the day, all sites observe a negative θ anomaly
303 throughout the UBL despite a negative q anomaly, indicating that sea breeze events during normal
304 days coincide with a cooler and drier daytime UBL. Sea breeze effects become apparent during the
305 mid-afternoon with the presence of a significant negative θ and positive q anomaly in the lower UBL,
306 with Staten Island experiencing effects first (approximately 16:00 LST) and the Bronx experiencing
307 effects last. It is worth noting that the q anomaly is weakest in the Bronx, indicating that the sea breeze
308 front weakens as it travels inland over New York City.

309

310 During extreme heat events, observations show that the sea breeze plays a moderating role on
311 surface conditions by reducing low-level temperatures and increasing low-level moisture content, similar
312 to phenomena observed during normal days. In Figure 29, the standardized anomalies of θ between
313 extreme heat days with and without a sea breeze are shown, averaged over all days. All sites shown
314 that extreme heat days with a sea breeze possess slightly higher values of θ in the mid-morning,
315 with significant low-level reduction in θ in the afternoon and evening. On average, the onset of the
316 low-level cooling occurs in Staten Island first at approximately 12:00 LST, with Queens following at
317 approximately 14:00 LST, and the Bronx at about 18:00 LST. This disparity in times appears to
318 represent the passage of the southeasterly sea breeze front through New York City, where the onset
319 time correlates with the distance from the New York Bight (Bornstein and Thompson, 1981). A similar
320 phenomenon is observed by the transport of q as shown in Figure 30, with drier conditions throughout
321 the UBL before 12:00 LST and increasing low-level moisture as the day progresses. With regards to
322 onset, q follows a similar pattern to θ in that the onset time is dependent from distance to the shore.
323 These anomalies present most significantly in the lowest 1000 m of the UBL after 12:00 LST, which
324 aligns with sea breeze circulation characteristics observed in Frizzola and Fisher (1963).

325 4.2 UBL dynamics during sea breeze events

326 Days with identifiable sea breeze events had lower U throughout the majority of the UBL, with the
327 most significant decreases during the nighttime, potentially due to the lessening of onshore flow due to
328 the reduction of the land-sea temperature gradient (Pullen et al., 2007), as shown in Figure 26. Vertical
329 motions, however, increased significantly in the Bronx and Queens during the late morning and early
330 afternoon, as shown in Figure 31. These anomalies likely indicate the increased presence of updrafts in
331 urbanized areas.

332

333 During days with identified sea breeze circulations, easterly winds increase in frequency in the
334 lower levels of the UBL, as shown in Figures 32, 33, and 34. Southeasterly winds (due to sea breezes
335 from the New York Bight) increased in frequency compared to all other days at all locations. The
336 occurrence frequency of southeasterly winds is correlated with the distance between the observation site
337 and the largest body of water in proximity of the metropolitan area (Atlantic Ocean), as Staten Island
338 reported 92.1% of all winds at 100 m as southeasterly between 12:00 and 20:00 LST (distance of 6.50 km
339 from Lower New York Bay), whereas Queens reported 67.4% (distance of 16.5 km), and Bronx reported
340 55.6% (distance of 32.9 km).

341

342 For sites near Long Island Sound (the Bronx and Queens), northeasterly winds increased in fre-
343 quency as well, though not to the same magnitude as southeasterly winds. This disparity in magnitude
344 suggests that the Long Island Sound sea breeze front is weaker than the New York Bight sea breeze
345 front, which aligns with previous studies of sea breeze fronts over New York City (Frizzola and Fisher,

346 1963; Meir et al., 2013).

347 5 Conclusions

- 348 • How do UBL structure and dynamics depart from the climatology during extreme heat events?
- 349 • How does the UBL structure impact the transport of scalars?
- 350 • The sea breeze reduces temperatures throughout the UBL after the onset of the sea breeze, which
- 351 typically occurs in the mid-afternoon in immediate coastal areas and in the evening for areas
- 352 further inland. The sea breeze also results in nocturnal low-level onshore moisture transport.

353 Acknowledgments

354 This research is made possible by the New York State (NYS) Mesonet. Original funding for the NYS
355 Mesonet was provided by Federal Emergency Management Agency grant FEMA-4085-DR-NY, with the
356 continued support of the NYS Division of Homeland Security & Emergency Services; the state of New
357 York; the Research Foundation for the State University of New York (SUNY); the University at Albany,
358 SUNY; the Atmospheric Sciences Research Center (ASRC) at SUNY Albany; and the Department of
359 Atmospheric and Environmental Sciences (DAES) at SUNY Albany.

360 References

- 361 Anderson, G Brooke and Michelle L Bell (2011). “Heat waves in the United States: mortality risk during heat
362 waves and effect modification by heat wave characteristics in 43 US communities”. In: *Environmental health
363 perspectives* 119.2, pp. 210–218.
- 364 Anurose, TJ, D Bala Subrahmanyam, and SV Sunilkumar (2018). “Two years observations on the diurnal
365 evolution of coastal atmospheric boundary layer features over Thiruvananthapuram (8.5° N, 76.9° E), India”.
366 In: *Theoretical and applied climatology* 131.1, pp. 77–90.
- 367 Arruda Moreira, Gregori de et al. (2020). “Study of the planetary boundary layer height in an urban environment
368 using a combination of microwave radiometer and ceilometer”. In: *Atmospheric Research* 240, p. 104932.
- 369 Banks, Robert F et al. (2015). “Performance evaluation of the boundary-layer height from lidar and the Weather
370 Research and Forecasting model at an urban coastal site in the north-east Iberian Peninsula”. In: *Boundary-
371 layer meteorology* 157.2, pp. 265–292.
- 372 Barlow, Janet F et al. (2011). “Boundary layer dynamics over London, UK, as observed using Doppler lidar
373 during REPARTEE-II”. In: *Atmospheric Chemistry and Physics* 11.5, pp. 2111–2125.
- 374 Black, Emily et al. (2004). “Factors contributing to the summer 2003 European heatwave”. In: *Weather* 59.8,
375 pp. 217–223.
- 376 Bornstein, Robert D and William T Thompson (1981). “Effects of frictionally retarded sea breeze and synoptic
377 frontal passages on sulfur dioxide concentrations in New York City”. In: *Journal of Applied Meteorology and
378 Climatology* 20.8, pp. 843–858.
- 379 Brotzge, Jerald A et al. (2020). “A technical overview of the new york state mesonet standard network”. In:
380 *Journal of Atmospheric and Oceanic Technology* 37.10, pp. 1827–1845.
- 381 Burillo, Daniel et al. (2019). “Electricity infrastructure vulnerabilities due to long-term growth and extreme heat
382 from climate change in Los Angeles County”. In: *Energy Policy* 128, pp. 943–953.
- 383 Chen, Feng, Xuchao Yang, and Weiping Zhu (2014). “WRF simulations of urban heat island under hot-weather
384 synoptic conditions: The case study of Hangzhou City, China”. In: *Atmospheric research* 138, pp. 364–377.
- 385 Chen, T C and J Alvin Kpaeyeh (1993). “The synoptic-scale environment associated with the low-level jet of the
386 Great Plains”. In: *Monthly weather review* 121.2, pp. 416–420.
- 387 Childs, Peter P and Sethu Raman (2005). “Observations and numerical simulations of urban heat island and sea
388 breeze circulations over New York City”. In: *Pure and Applied Geophysics* 162.10, pp. 1955–1980.
- 389 Colle, Brian A and David R Novak (2010). “The New York Bight jet: climatology and dynamical evolution”. In:
390 *Monthly Weather Review* 138.6, pp. 2385–2404.

- 391 Dong, Li et al. (2018). "The dynamical linkage of atmospheric blocking to drought, heatwave and urban heat
392 island in southeastern US: A multi-scale case study". In: *Atmosphere* 9.1, p. 33.
- 393 Forzieri, Giovanni et al. (2018). "Escalating impacts of climate extremes on critical infrastructures in Europe".
394 In: *Global environmental change* 48, pp. 97–107.
- 395 Frizzola, John A and Edwin L Fisher (1963). "A series of sea breeze observations in the New York City area".
396 In: *Journal of Applied Meteorology and Climatology* 2.6, pp. 722–739.
- 397 Frumkin, Howard (2016). "Urban sprawl and public health". In: *Public health reports*.
- 398 Gedzelman, SD et al. (2003). "Mesoscale aspects of the urban heat island around New York City". In: *Theoretical
399 and applied climatology* 75.1, pp. 29–42.
- 400 Grund, Christian J et al. (2001). "High-resolution Doppler lidar for boundary layer and cloud research". In:
401 *Journal of Atmospheric and Oceanic Technology* 18.3, pp. 376–393.
- 402 Güldner, J and D Spänkuch (2001). "Remote sensing of the thermodynamic state of the atmospheric boundary
403 layer by ground-based microwave radiometry". In: *Journal of Atmospheric and Oceanic Technology* 18.6,
404 pp. 925–933.
- 405 Heaviside, Clare, Helen Macintyre, and Sotiris Vardoulakis (2017). "The urban heat island: implications for health
406 in a changing environment". In: *Current environmental health reports* 4.3, pp. 296–305.
- 407 Hewison, Tim and Catherine Gaffard (2003). "Radiometrics MP3000 microwave radiometer performance assess-
408 ment". In: *Obs. Development Technical Report TR29, Met Office, National Meteorological Library, Exeter,
409 UK. Also available from <http://tim.hewison.org/TR29.pdf>*.
- 410 Hrisko, Joshua, Prathap Ramamurthy, and Jorge E Gonzalez (2021). "Estimating heat storage in urban areas
411 using multispectral satellite data and machine learning". In: *Remote Sensing of Environment* 252, p. 112125.
- 412 Hu, Xiao-Ming and Ming Xue (2016). "Influence of synoptic sea-breeze fronts on the urban heat island intensity
413 in Dallas–Fort Worth, Texas". In: *Monthly Weather Review* 144.4, pp. 1487–1507.
- 414 Ignatov, A et al. (2010). "GOES-R Advanced Baseline Imager (ABI) algorithm theoretical basis document for
415 sea surface temperature". In: *NOAA NESDIS Center for Satellite Applications and Research*.
- 416 Jiang, Shaojing et al. (2019). "Amplified urban heat islands during heat wave periods". In: *Journal of Geophysical
417 Research: Atmospheres* 124.14, pp. 7797–7812.
- 418 Kumer, Valerie-M, Joachim Reuder, and Birgitte R Furevik (2014). "A comparison of LiDAR and radiosonde
419 wind measurements". In: *Energy Procedia* 53, pp. 214–220.
- 420 Li, Dan and Elie Bou-Zeid (2013). "Synergistic interactions between urban heat islands and heat waves: The
421 impact in cities is larger than the sum of its parts". In: *Journal of Applied Meteorology and Climatology* 52.9,
422 pp. 2051–2064.
- 423 Luo, Bingkun and Peter J Minnett (2021). "Skin Sea Surface Temperatures From the GOES-16 ABI Validated
424 With Those of the Shipborne M-AERI". In: *IEEE Transactions on Geoscience and Remote Sensing* 59.12,
425 pp. 9902–9913.
- 426 Madrigano, Jaime et al. (2015). "A case-only study of vulnerability to heat wave-related mortality in New York
427 City (2000–2011)". In: *Environmental health perspectives* 123.7, pp. 672–678.
- 428 McEvoy, Darryn, Iftekhar Ahmed, and Jane Mullett (2012). "The impact of the 2009 heat wave on Melbourne's
429 critical infrastructure". In: *Local Environment* 17.8, pp. 783–796.
- 430 Meir, Talmor et al. (2013). "Forecasting the New York City urban heat island and sea breeze during extreme
431 heat events". In: *Weather and Forecasting* 28.6, pp. 1460–1477.
- 432 Melecio-Vázquez, David et al. (2018). "Thermal Structure of a Coastal–Urban Boundary Layer". In: *Boundary-
433 Layer Meteorology* 169 (1), pp. 151–161. ISSN: 15731472.
- 434 Miller, STK et al. (2003). "Sea breeze: Structure, forecasting, and impacts". In: *Reviews of geophysics* 41.3.
- 435 Miralles, Diego G et al. (2014). "Mega-heatwave temperatures due to combined soil desiccation and atmospheric
436 heat accumulation". In: *Nature geoscience* 7.5, pp. 345–349.
- 437 National Weather Service, NOAA (May 2018). *National Weather Service New York, NY excessive heat page*. URL:
438 <https://www.weather.gov/okx/excessiveheat>.
- 439 NOAA et al. (1998). *Automated Surface Observing System (ASOS) User's Guide*. URL: <https://www.weather.gov/media/asos/aum-toc.pdf>.
- 440 Pelliccioni, A et al. (2012). "Some characteristics of the urban boundary layer above Rome, Italy, and applicability
441 of Monin–Obukhov similarity". In: *Environmental fluid mechanics* 12.5, pp. 405–428.
- 443 Peng, Roger D et al. (2011). "Toward a quantitative estimate of future heat wave mortality under global climate
444 change". In: *Environmental health perspectives* 119.5, pp. 701–706.

- 445 Pullen, Julie et al. (2007). "Atmospheric response to local upwelling in the vicinity of New York–New Jersey
446 harbor". In: *Journal of applied meteorology and climatology* 46.7, pp. 1031–1052.
- 447 Quan, Jiannong et al. (2013). "Evolution of planetary boundary layer under different weather conditions, and its
448 impact on aerosol concentrations". In: *Particuology* 11.1, pp. 34–40.
- 449 Ramamurthy, P and E Bou-Zeid (2017). "Heatwaves and urban heat islands: a comparative analysis of multiple
450 cities". In: *Journal of Geophysical Research: Atmospheres* 122.1, pp. 168–178.
- 451 Ramamurthy, P, D Li, and E Bou-Zeid (2017). "High-resolution simulation of heatwave events in New York
452 City". In: *Theoretical and applied climatology* 128.1, pp. 89–102.
- 453 Ramamurthy, Prathap and E Bou-Zeid (2014). "Contribution of impervious surfaces to urban evaporation". In:
454 *Water Resources Research* 50.4, pp. 2889–2902.
- 455 Robinson, Peter J (2001). "On the definition of a heat wave". In: *Journal of Applied Meteorology and Climatology*
456 40.4, pp. 762–775.
- 457 Rose, Thomas et al. (2005). "A network suitable microwave radiometer for operational monitoring of the cloudy
458 atmosphere". In: *Atmospheric research* 75.3, pp. 183–200.
- 459 Sánchez, JL et al. (2013). "A method to improve the accuracy of continuous measuring of vertical profiles of
460 temperature and water vapor density by means of a ground-based microwave radiometer". In: *Atmospheric
461 Research* 122, pp. 43–54.
- 462 Shrestha, Bhupal et al. (2021). "Overview and Applications of the New York State Mesonet Profiler Network".
463 In: *Journal of Applied Meteorology and Climatology* 60.11, pp. 1591–1611.
- 464 Stéfanon, Marc et al. (2014). "Soil moisture-temperature feedbacks at meso-scale during summer heat waves over
465 Western Europe". In: *Climate dynamics* 42.5, pp. 1309–1324.
- 466 Tewari, Mukul et al. (2019). "Interaction of urban heat islands and heat waves under current and future climate
467 conditions and their mitigation using green and cool roofs in New York City and Phoenix, Arizona". In:
468 *Environmental Research Letters* 14.3, p. 034002.
- 469 Thomas, Natalie P et al. (2020). "Mechanisms associated with daytime and nighttime heat waves over the
470 contiguous united states". In: *Journal of Applied Meteorology and Climatology* 59.11, pp. 1865–1882.
- 471 Thompson, William T, Teddy Holt, and Julie Pullen (2007). "Investigation of a sea breeze front in an urban envi-
472 ronment". In: *Quarterly Journal of the Royal Meteorological Society: A journal of the atmospheric sciences,
473 applied meteorology and physical oceanography* 133.624, pp. 579–594.
- 474 Wang, Z et al. (2012). "Lidar measurement of planetary boundary layer height and comparison with microwave
475 profiling radiometer observation". In: *Atmospheric Measurement Techniques* 5.8, pp. 1965–1972.
- 476 Wu, Yonghua et al. (2019). "Observation of heat wave effects on the urban air quality and PBL in New York
477 City area". In: *Atmospheric Environment* 218, p. 117024.
- 478 Yu, Yunyue et al. (2008). "Developing algorithm for operational GOES-R land surface temperature product". In:
479 *IEEE Transactions on Geoscience and Remote Sensing* 47.3, pp. 936–951.
- 480 Zhang, Da-Lin, Yi-Xuan Shou, and Russell R Dickerson (2009). "Upstream urbanization exacerbates urban heat
481 island effects". In: *Geophysical Research Letters* 36.24.
- 482 Zhang, Yuanjie et al. (2020). "Aircraft observed diurnal variations of the planetary boundary layer under heat
483 waves". In: *Atmospheric Research* 235, p. 104801.
- 484 Zhao, Lei et al. (2018). "Interactions between urban heat islands and heat waves". In: *Environmental research
485 letters* 13.3, p. 034003.
- 486 Zuo, Jian et al. (2015). "Impacts of heat waves and corresponding measures: a review". In: *Journal of Cleaner
487 Production* 92, pp. 1–12.

488 Appendix

$$p = p_0 \exp \frac{-gz}{RT_0}$$

$$\theta = T \left(\frac{p_0}{p} \right)^{\frac{R}{cp}}$$

$$q = \frac{w}{1+w} = \frac{\frac{\varepsilon \rho'_v R_v T}{p - \rho'_v R_v T}}{1 + \frac{\varepsilon \rho'_v R_v T}{p - \rho'_v R_v T}}$$

489

$$Ri_b = \frac{g\Delta\bar{\theta}_v\Delta z}{\bar{\theta}_v [(\Delta\bar{U}^2) + (\Delta\bar{V}^2)]}$$

Table 2: Symbols and abbreviations used in the paper.

Symbol/Abbreviation	Definition
σ	Standard deviation
θ	Potential temperature
q	Specific humidity
U	Horizontal wind speed
w	Vertical velocity
UBL	Urban boundary layer
MLH	Mixed layer height

490

Figures

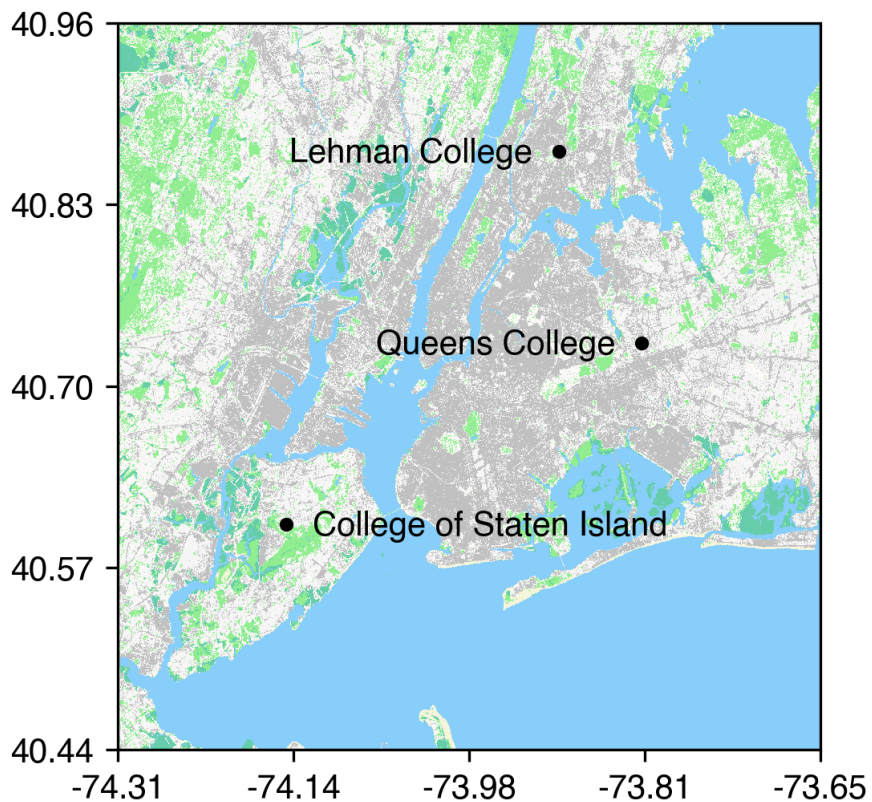


Figure 1: Observation sites overlaid on NLCD land cover types..

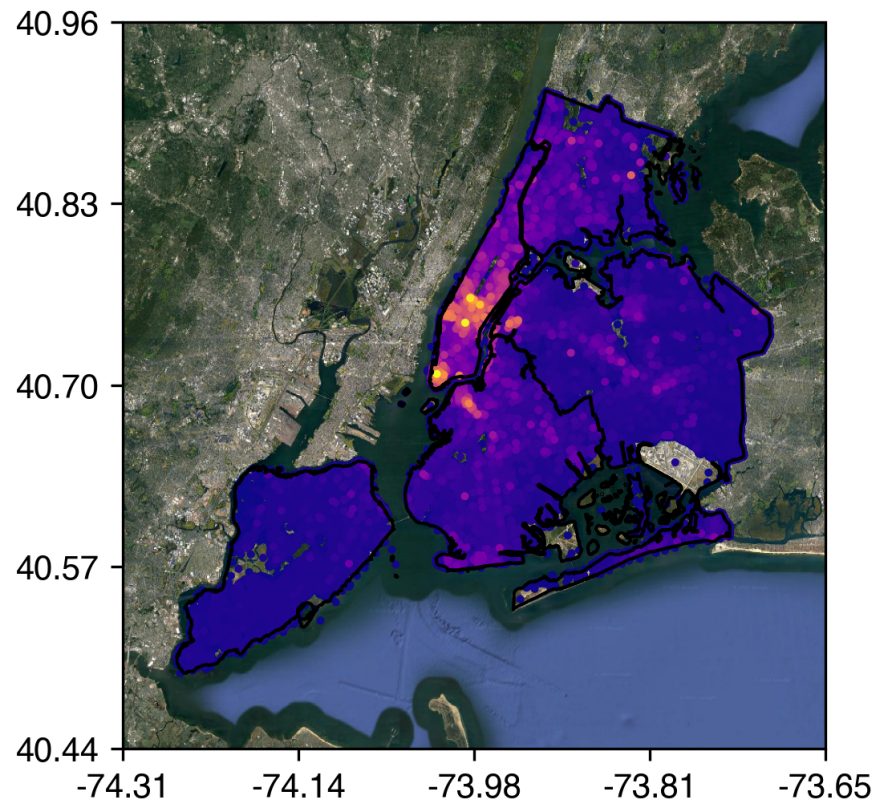


Figure 2: Building heights in New York City. Taken from NYC DOB data.

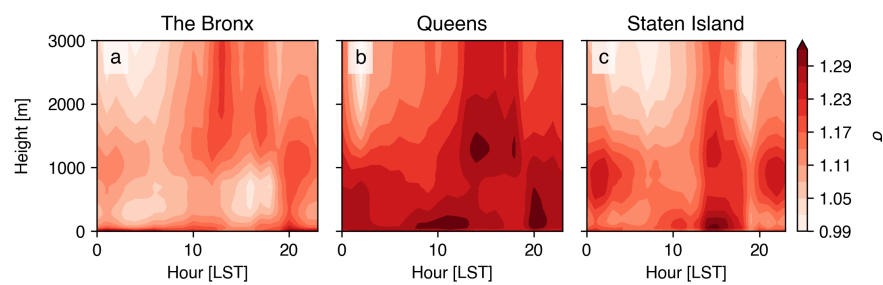


Figure 3: Anomalies of θ during extreme heat events relative to the climatology over the urban boundary layer.

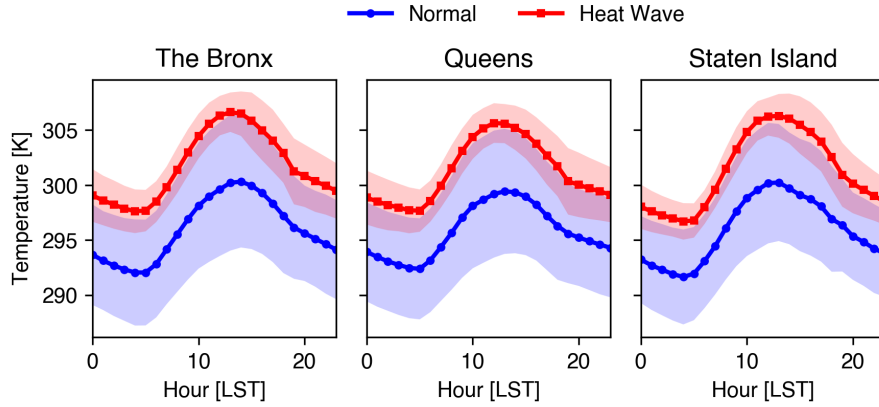


Figure 4: Anomalies of temperature during extreme heat events relative to the climatology at the surface.

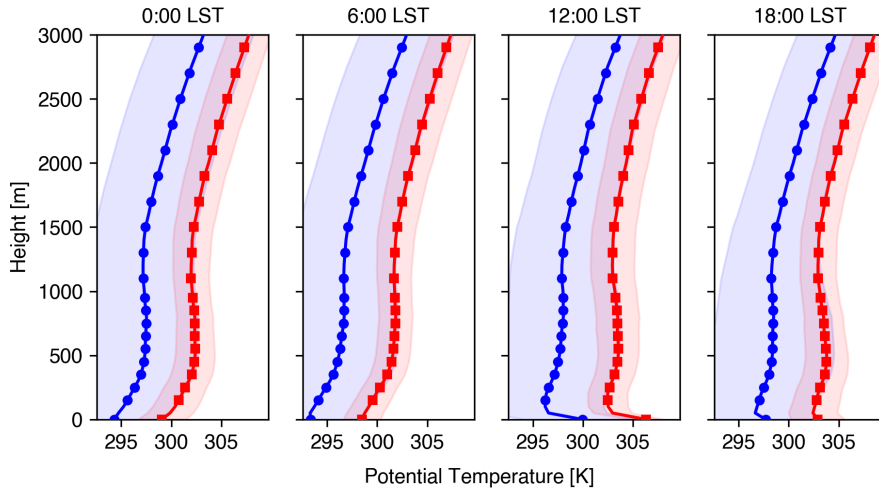


Figure 5: Vertical profiles of θ in the Bronx during normal days (blue) and extreme heat events (red).

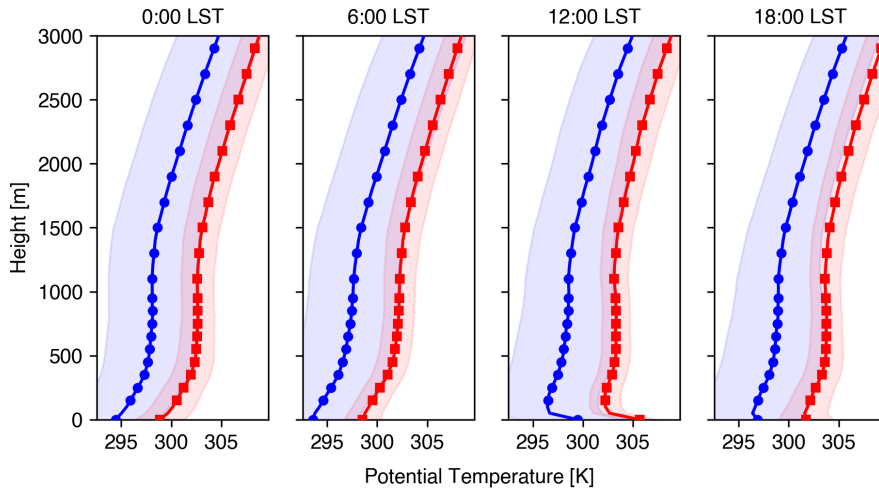


Figure 6: Vertical profiles of θ in Queens during normal days (blue) and extreme heat events (red).

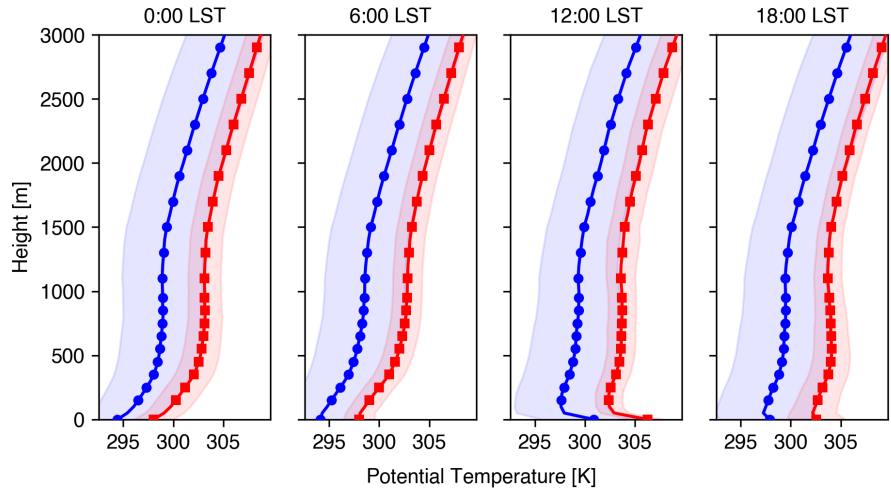


Figure 7: Vertical profiles of θ in Staten Island during normal days (blue) and extreme heat events (red).

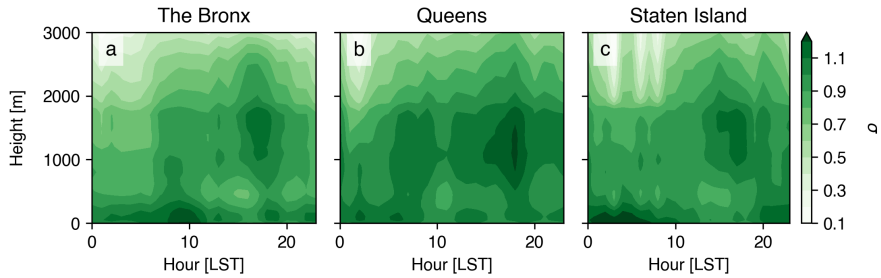


Figure 8: Anomalies of q during extreme heat events relative to the climatology over the urban boundary layer.

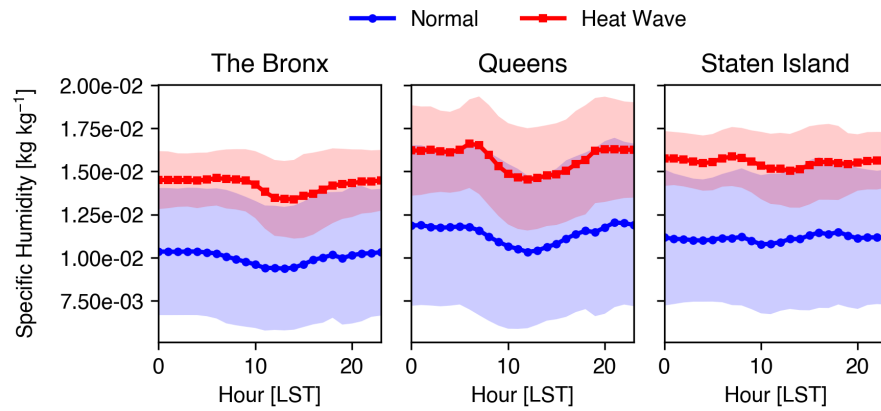


Figure 9: Anomalies of q during extreme heat events relative to the climatology at the surface.

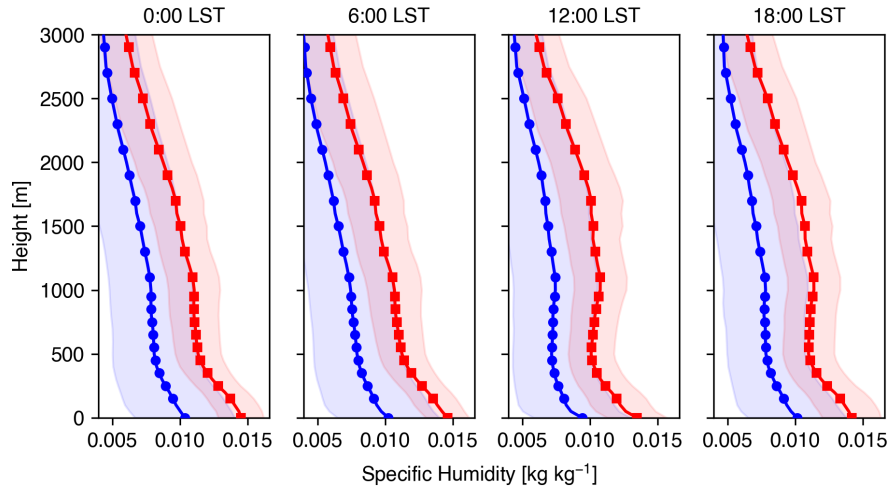


Figure 10: Vertical profiles of q in the Bronx during normal days (blue) and extreme heat events (red).

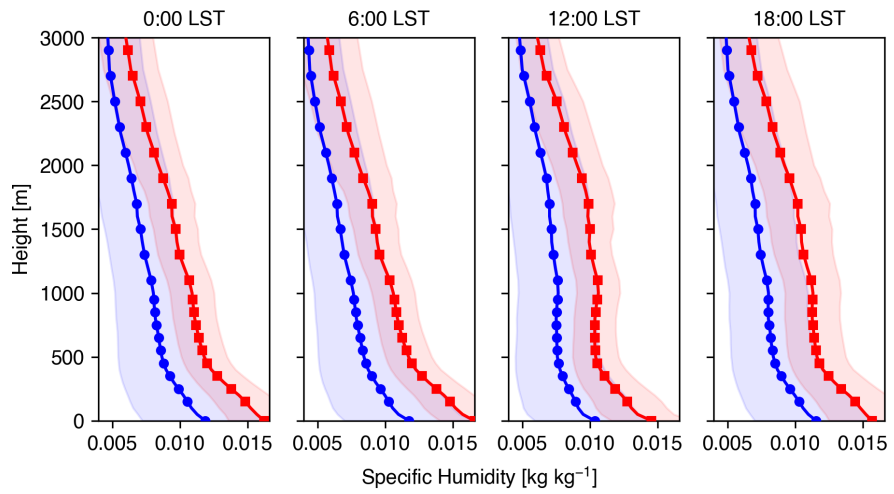


Figure 11: Vertical profiles of q in Queens during normal days (blue) and extreme heat events (red).

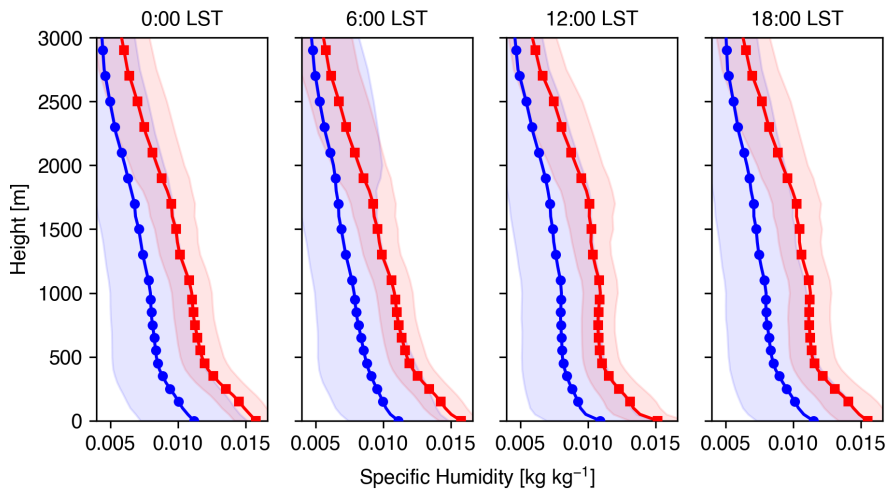


Figure 12: Vertical profiles of q in Staten Island during normal days (blue) and extreme heat events (red).

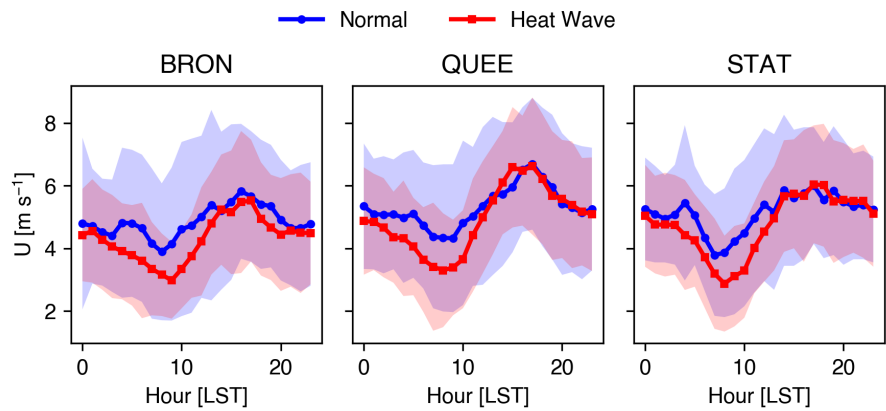


Figure 13: Anomalies of low-level U during extreme heat events relative to the climatology.

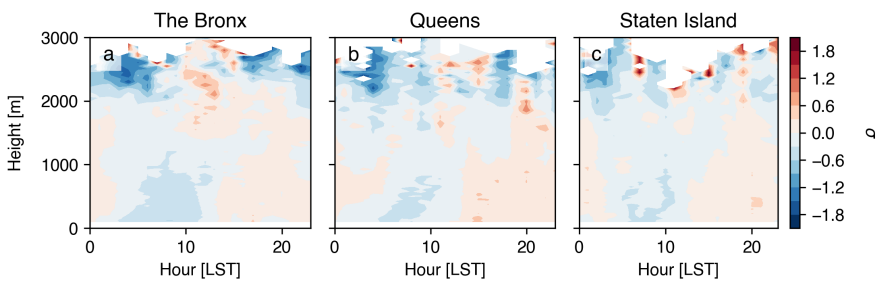


Figure 14: Anomalies of U during extreme heat events relative to the climatology over the urban boundary layer.

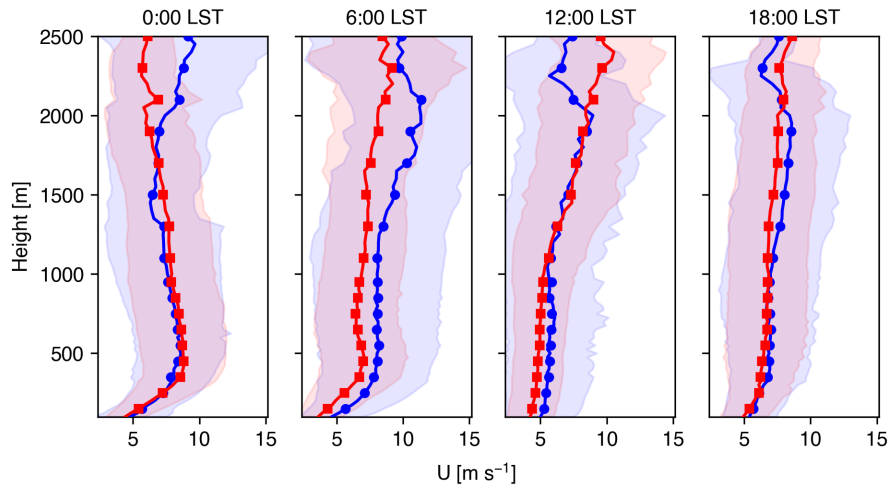


Figure 15: Vertical profiles of U in the Bronx during normal days (blue) and extreme heat events (red).

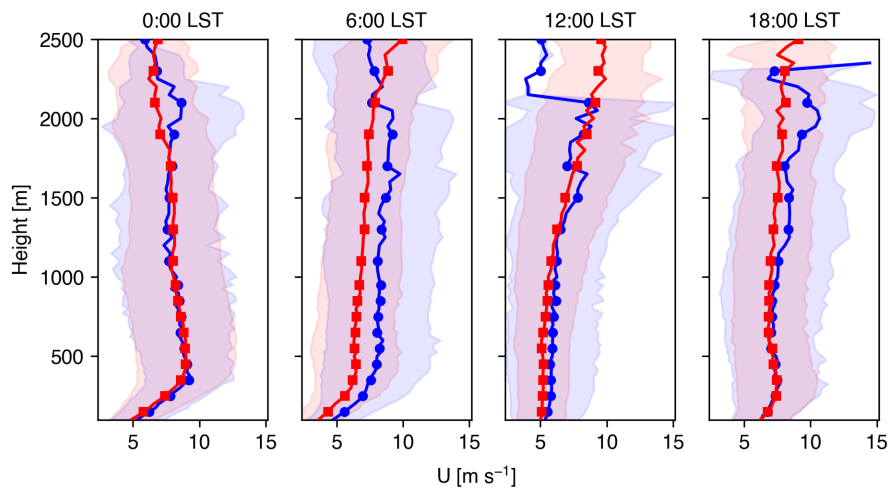


Figure 16: Vertical profiles of U in Queens during normal days (blue) and extreme heat events (red).

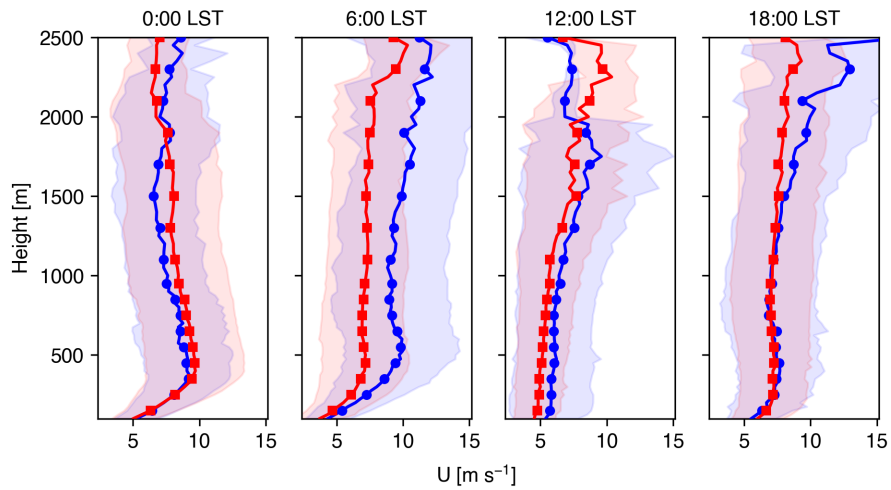


Figure 17: Vertical profiles of U in Staten Island during normal days (blue) and extreme heat events (red).

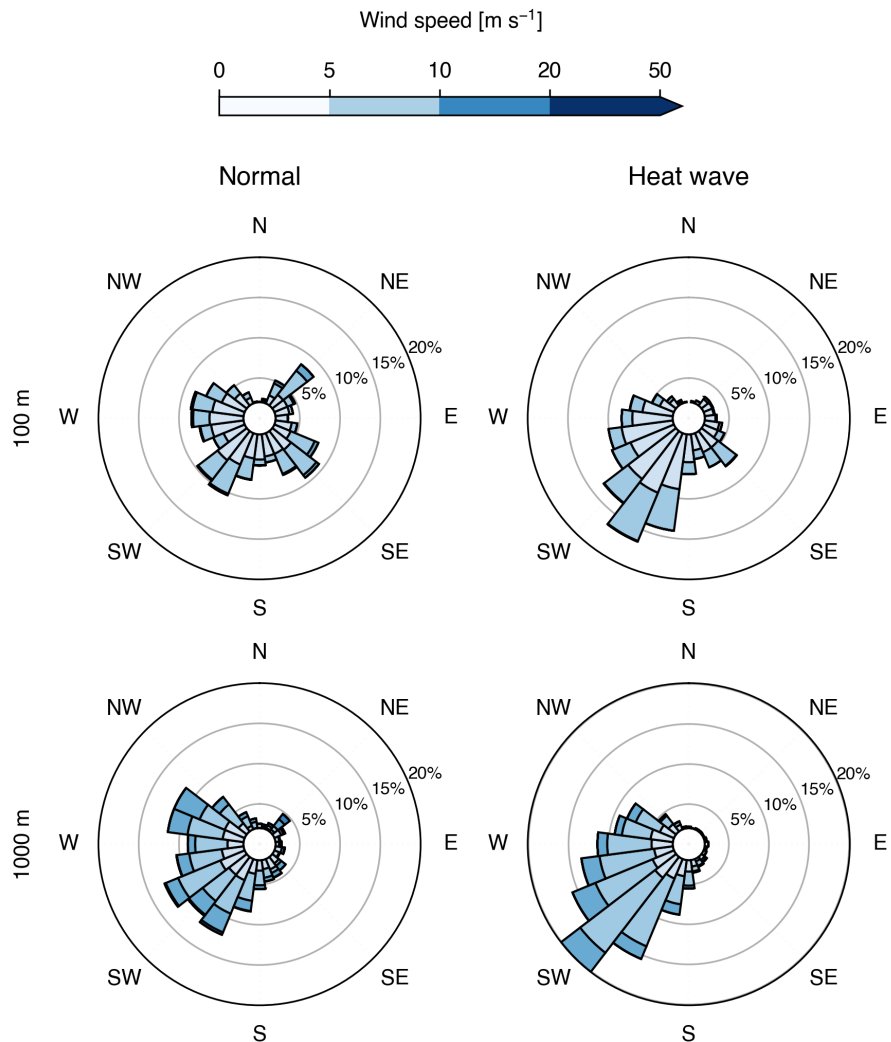


Figure 18: Horizontal winds in the lower-level (100 m) and mid-level of the urban boundary layer over the Bronx.

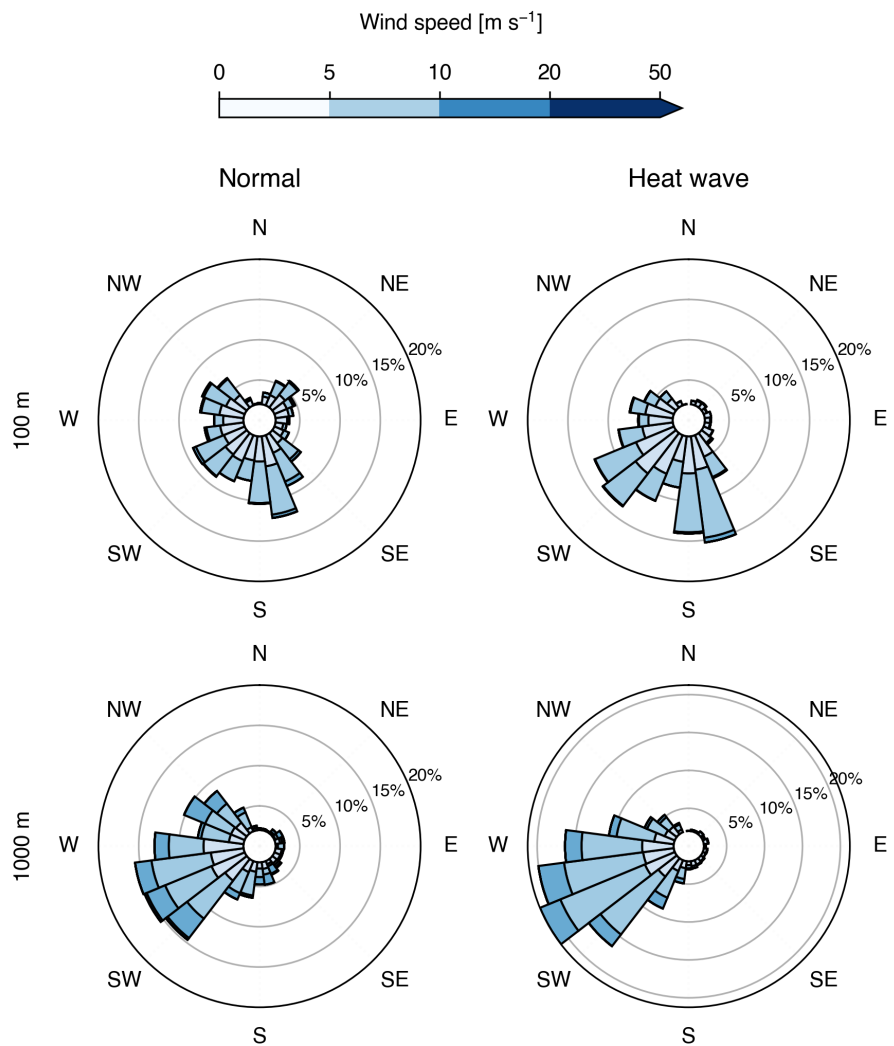


Figure 19: Horizontal winds in the lower-level (100 m) and mid-level of the urban boundary layer over Queens.

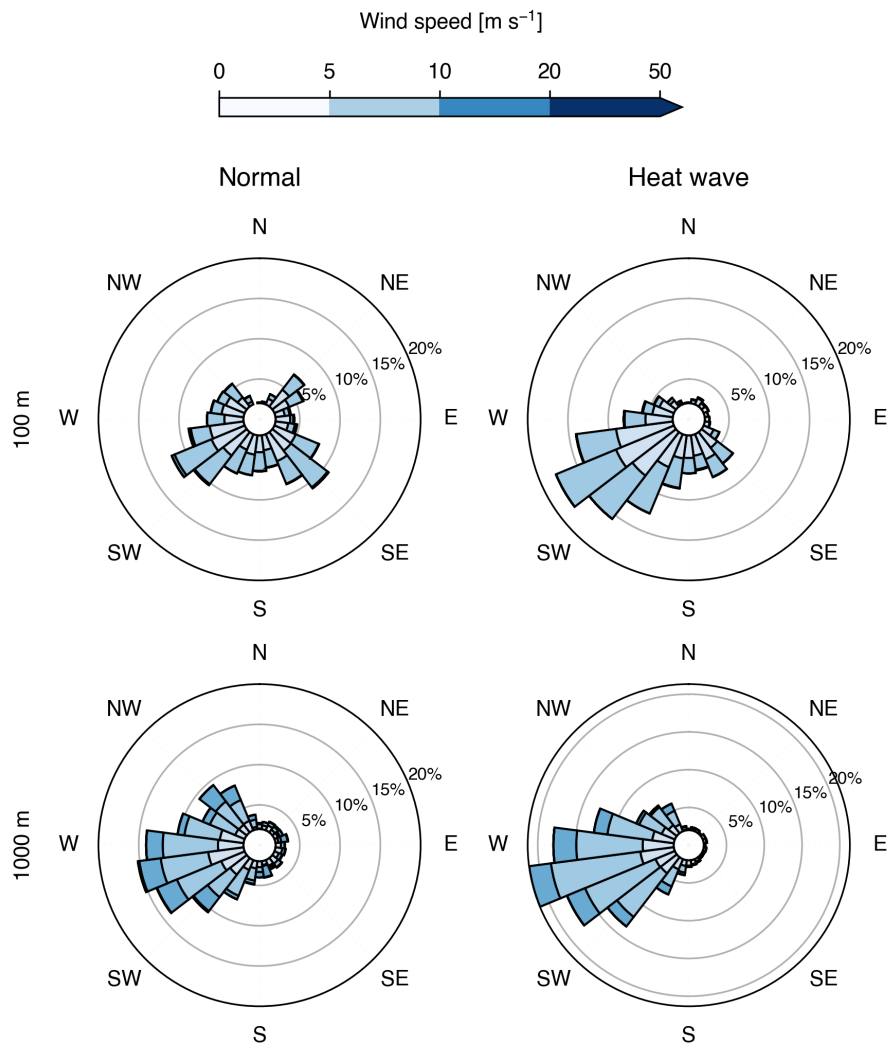


Figure 20: Horizontal winds in the lower-level (100 m) and mid-level of the urban boundary layer over Staten Island.

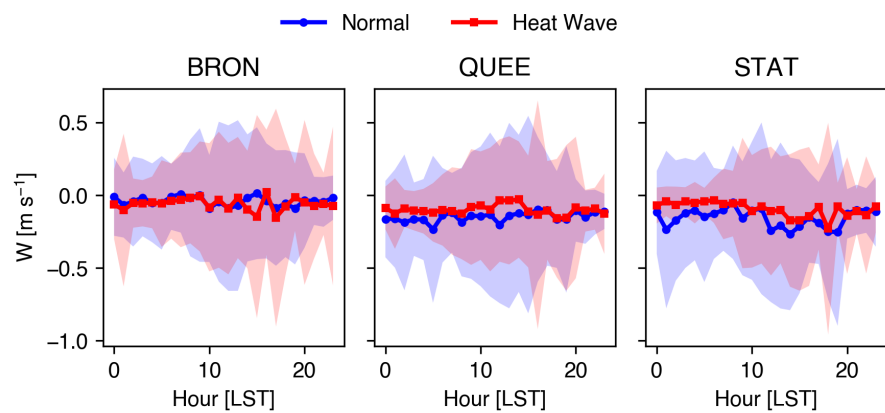


Figure 21: Anomalies of low-level w during extreme heat events relative to the climatology.

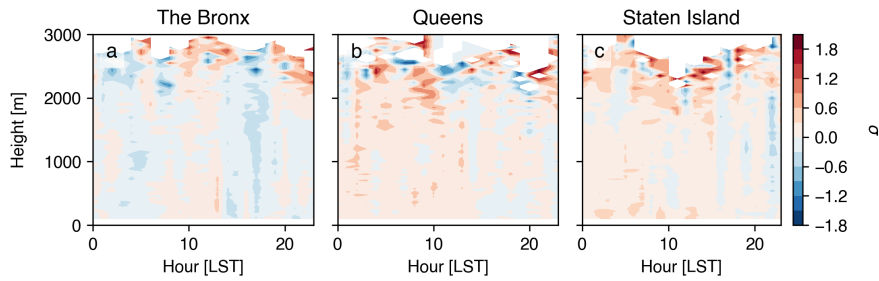


Figure 22: Anomalies of w during extreme heat events relative to the climatology over the urban boundary layer.

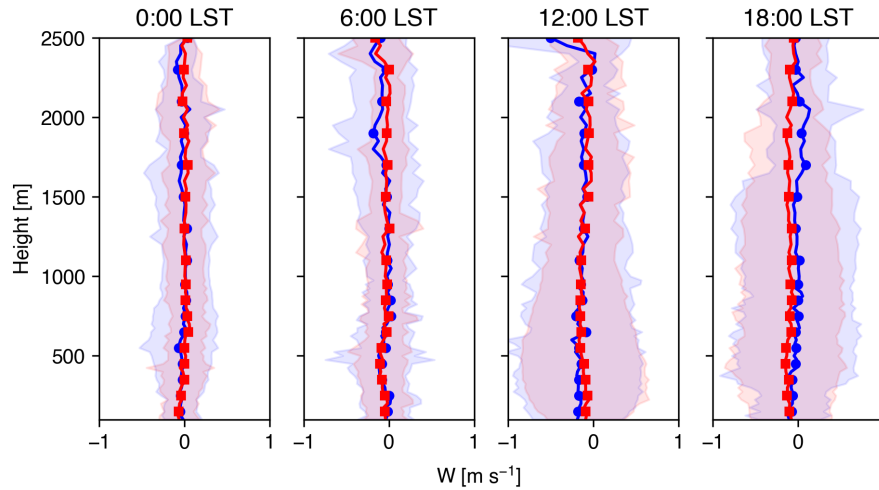


Figure 23: Vertical profiles of w in the Bronx during normal days (blue) and extreme heat events (red).

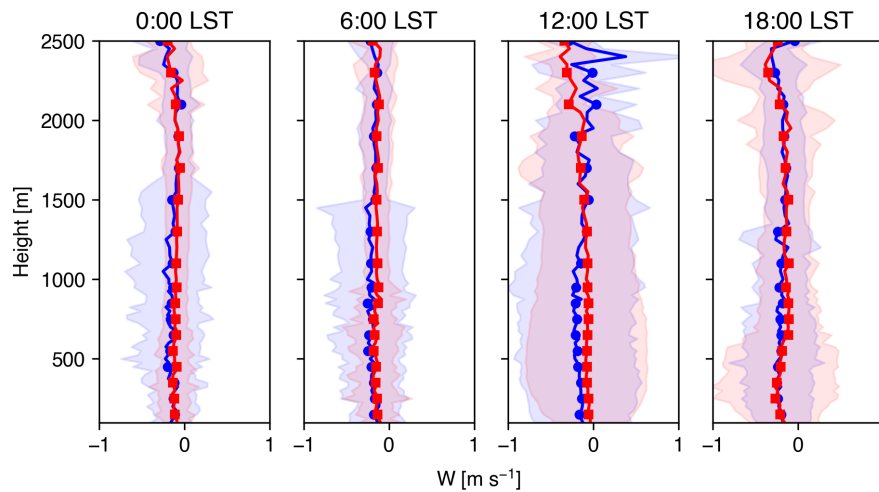


Figure 24: Vertical profiles of w in Queens during normal days (blue) and extreme heat events (red).

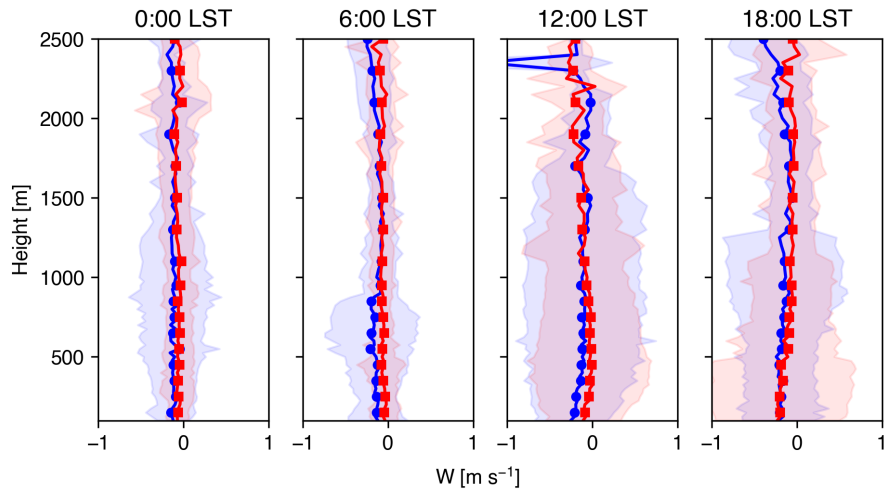


Figure 25: Vertical profiles of U in Staten Island during normal days (blue) and extreme heat events (red).

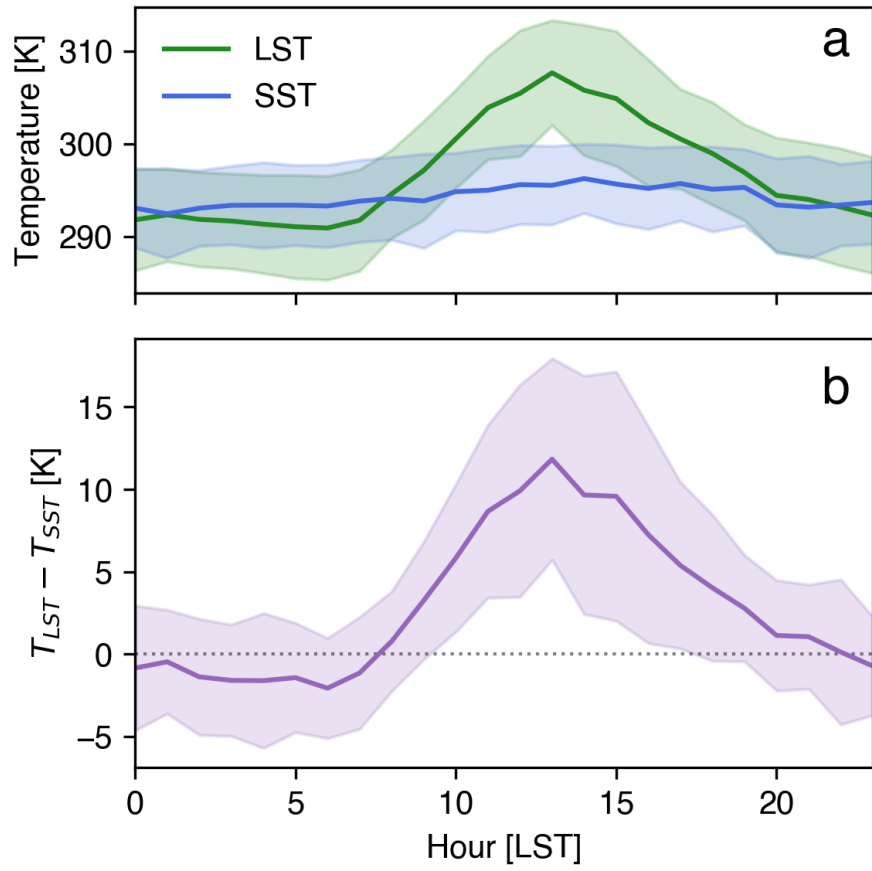


Figure 26: Temperature difference between Queens and New York Bight.

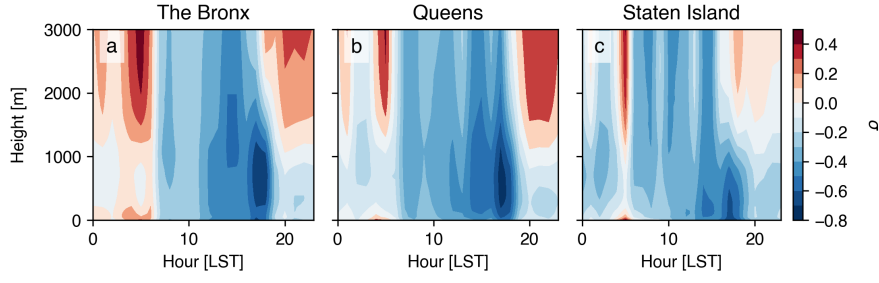


Figure 27: Anomalies of θ for normal days with a sea breeze relative to normal days without a sea breeze.

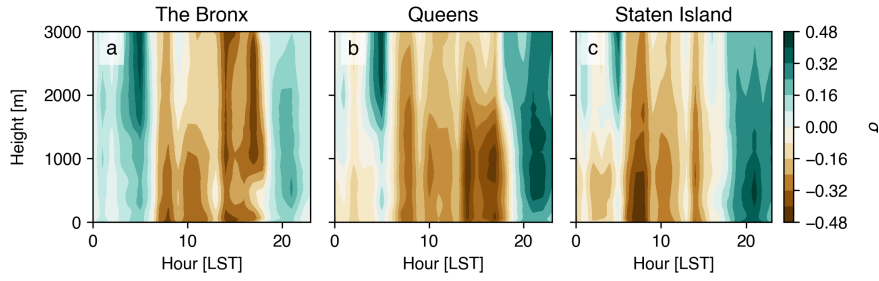


Figure 28: Anomalies of q for normal days with a sea breeze relative to normal days without a sea breeze.

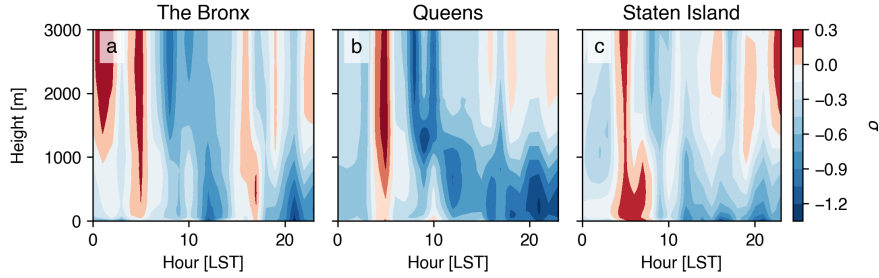


Figure 29: Anomalies of θ for heat wave days with a sea breeze relative to heat wave days without a sea breeze.

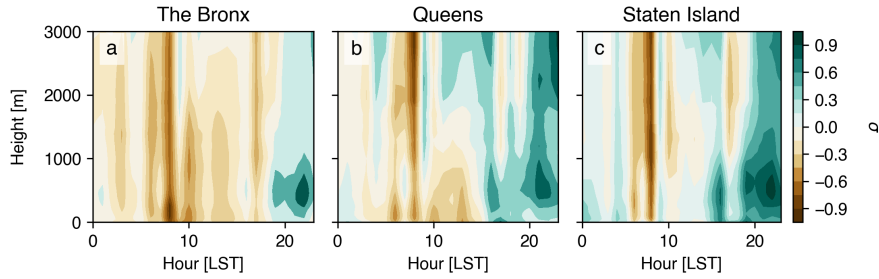


Figure 30: Anomalies of q for heat wave days with a sea breeze relative to heat wave days without a sea breeze.

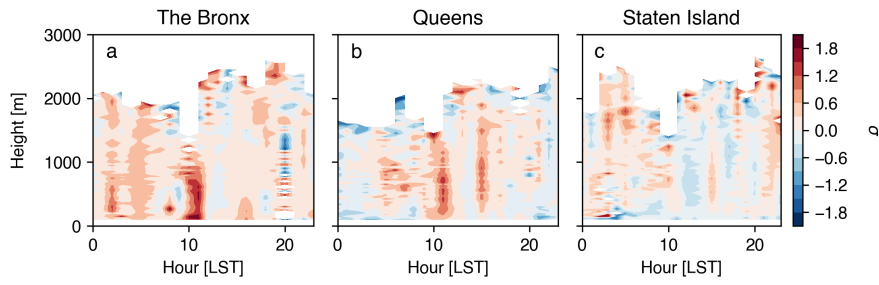


Figure 31: Anomalies of w for heat wave days with a sea breeze relative to heat wave days without a sea breeze.

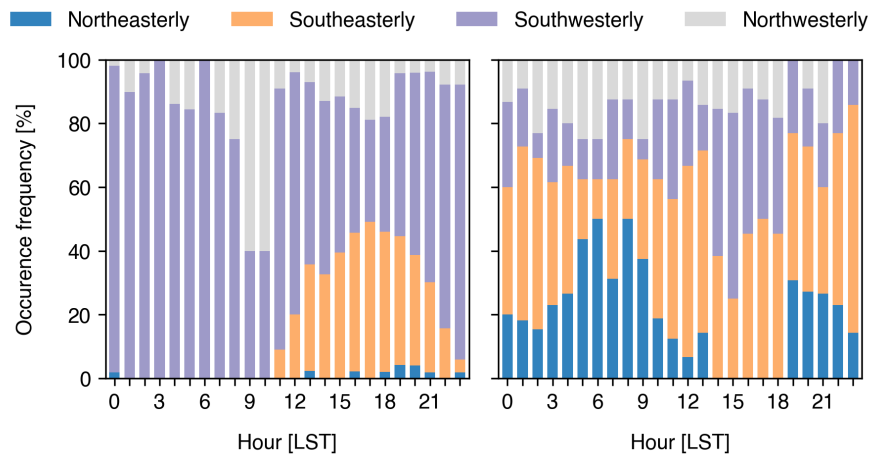


Figure 32: Occurrence frequency of wind directions at 100 m in the Bronx.

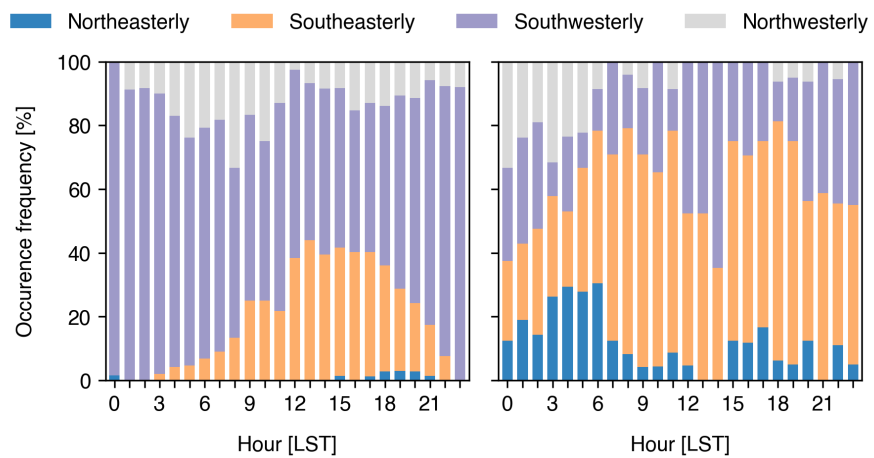


Figure 33: Occurrence frequency of wind directions at 100 m in Queens.

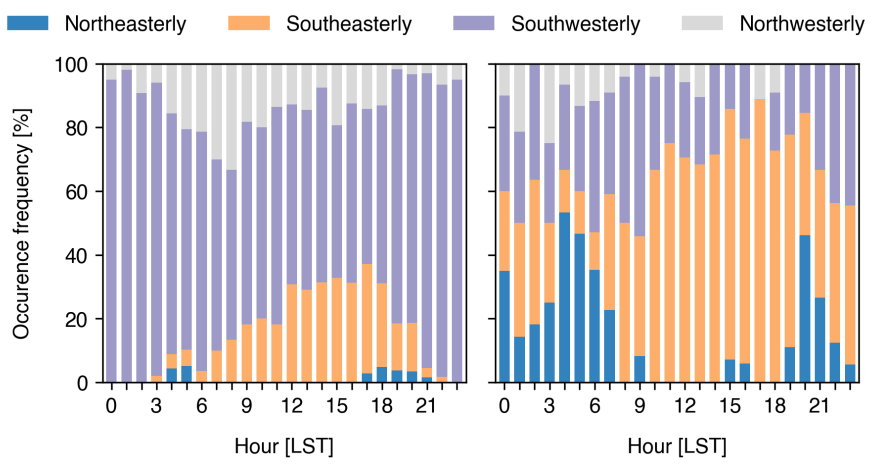


Figure 34: Occurrence frequency of wind directions at 100 m in Staten Island.